Thermogravimetric analysis-mass spectrometry (TG-MS) of selected Chinese kaolinites

Hongfei Cheng [a,b,c], Jing Yang [c], Qinfu Liu [a], Junkai He [a], Ray L. Frost [c•]

[a] School of Geoscience and Surveying Engineering, China University of Mining & Technology, Beijing, 100083 China

[b] School of Mining Engineering, Inner Mongolia University of Science & Technology, Baotou 014010 China

[c] Chemistry Discipline, Faculty of Science and Technology, Queensland University of Technology, 2 George Street, GPO Box 2434, Brisbane, Queensland 4001, Australia

Abstract: Thermogravimetric analysis-mass spectrometry, X-ray diffraction and scanning electron microscopy (SEM) were used to characterize eight kaolinite samples from China. The results show that the thermal decomposition occurs in three main steps (a) desorption of water below 100 °C, (b) dehydration at about 225 °C, (c) well defined dehydroxylation at around 450 °C. It is also found that decarbonization took place at 710 °C due to the decomposition of calcite impurity in kaolin. The temperature of dehydroxylation of kaolinite is found to be influenced by the degree of disorder of the kaolinite structure and the gases evolved in the decomposition process can be various because of the different amount and kinds of impurities. It is evident by the mass spectra that the interlayer carbonate from impurity of calcite and organic carbon is released as CO_2 around 225, 350 and 710 °C in the kaolinite samples.

Keywords: Thermogravimetry; Kaolinite; Halloysite; Mass spectrometry

• Author to whom correspondence should be addressed (r.frost@qut.edu.au)

1. Introduction

Kaolin, relatively pure clay, has a wide variety of applications in industry, particularly as paper filler, rubber filler and coating pigment [1-5]. Kaolin is rock comprised largely of the kaolin group mineral including kaolinite, halloysite, dickite and nacrite. The most common kaolin mineral is kaolinite, which has attracted much attention over a long period of time [5-9]. The last two members of the kaolin group are relatively rare, although significant deposits of halloysite are known [4, 10].

Kaolinite, $Al_2[Si_2O_5](OH)_4$ is a naturally occurring inorganic polymer with a layer structure consisting of siloxane and gibbsite-like layers. The siloxane layer is composed of SiO_4 tetrahedra linked in a hexagonal array. The bases of the tetrahedra are approximately coplanar and the apical oxygen atoms are linked to a second layer containing aluminum ions and OH groups (the gibbsite-type layer). Halloysite occurs mainly in two different polymorphs, the hydrated form (basal distance around 10 Å) with the minimal formula of $Al_2Si_2O_5(OH)_4 \cdot 2H_2O$, and the dehydrated form (basal distance around 7 Å) with the minimal formula of $Al_2Si_2O_5(OH)_4$, being identical to kaolinite. The hydrated form converts irreversibly into the dehydrated form when dried at temperatures below 100 °C [11, 12]. This halloysite(d=10Å) easily dehydrates in atmospheric pressures at temperatures around 60 °C or in vacuum at room temperature. This anhydrous form has a basal spacing near 7.2 Å and is metastable, recovering its interlayer water when placed in wet air. Because the 1:1 layers in hydrated halloysite are separated from each other by a water layer and occur in a scroll-like morphology, halloysite has a larger cation exchange capacity and surface area than kaolinite [11, 13, 14].

The industrial application of kaolin or China clay are diverse and depend largely on the physical properties, such as whiteness, platyness, particle size, etc. specific for each kaolin deposit [15]. However, most of the industrial kaolin in china which generally contain a certain amount of organic carbon must be calcined to improve whiteness [16, 17]. The calcined kaolin is often used in the rubber and plastic, ceramic raw material, fiberglass, cracking catalysts, cosmetics, medicines and other polymers [18-20]. Thermal stability and whiteness are very important properties of calcined kaolin particularly for industrial applications [2, 21]. The thermal transformation of kaolinite and halloysite is a very important step, which has been investigated by Brown et al. 1985 [22, 23], He et al. 1995 [24] and others [25-30]. The mechanisms of dehydroxylation of kaolinite also have been studied [25, 28]. Interest in such minerals and their thermal stability rests with the possible identification of these

minerals for new directions in industrial applications. Though kaolin has been used for many years and in many fields, to explore the complexities involved in its phase transformation and microstructural evolution at elevated temperature is still a challenging task [31]. Thus, the more detailed investigations are necessary to determine the influencing factor in dehydroxylation at the elevated temperature among the several kaolinite polytypes.

Thermal analysis using thermogrvimetric techniques enables the mass loss steps, the temperature of the mass loss and the mechanism for the mass loss to be determined [32]. It has proven extremely useful for determining the stability of minerals. Thermogravimetic-mass spectrometry methods can provide the composition of minerals [13, 33-35]. In the current study, to the best of the authors knowledge no thermoanalytical studies and evolved gases analysis of kaolinite for geosequestration of greenhouses and influencing factor in dehydroxylation have been undertaken; although differential thermal analysis of some related minerals has been published [36-39]. This paper reports the thermal analysis of eight kaolins from China using XRD, TG-MS and SEM.

2. Experimental methods

2.1 Materials

Eight kaolin samples, including six kaolinites and two halloysites, were selected for this study (Table 1). The samples were used directly, without prior size fraction separation, since one of the objectives was to determine the influence on the degree of order of the particle size of the several samples.

2.2 X-ray diffraction

X-ray diffraction patterns were collected using a PANalytical X'Pert PRO X-ray diffractometer (radius: 240.0 mm). Incident X-ray radiation was produced from a line focused PW3373/10 Cu X-ray tube, operating at 40 kV and 40 mA, with Cu Kα radiation of 1.540596 Å. The incident beam passed through a 0.04 rad soller slit, a 1/2 ° divergence slit, a 15 mm fixed mask, and a 1 ° fixed antiscatter slit.

2.3 Thermogravimetric analysis and mass spectrometry

Thermogravimetric analysis (TG) of the samples was carried out with a TA® Instruments incorporated high-resolution thermogravimetric analyser (series Q500) in a flowing nitrogen atmosphere (60 cm^3min^{-1}). Approximately 50 mg of each sample underwent thermal analysis, with a heating rate of 5 °C/min, with resolution of 6 from 25 °C to 1000 °C. With the isothermal, isobaric heating program of the instrument the furnace temperature was regulated precisely to provide a uniform rate of decomposition in the main decomposition stage. The TG instrument was coupled to a Balzers (Pfeiffer) mass spectrometer for gas analysis. Only water vapour, carbon, sulfur dioxide and oxygen were analysed. In the MS figures, e.g. Fig. 3, a background of broad peaks may be observed. This background occurs for all the ion current curves. The background becomes more prominent as the scale expansion is increased. It is considered that this background may be due to sublimation of chemicals deposited in the capillary which connects the TA instrument to the MS.

2.4 Scanning electron microscopy (SEM)

The morphology of kaolin particles was observed by using a scanning electron microscope (SEM), Hitachi S-4800. Samples were coated with a gold/palladium film and the SEM-images were obtained using a secondary electron detector.

3. Results and discussion

3.1 X-ray diffraction (XRD) and chemical composition

The XRD patterns of these eight kaolin samples together with standard XRD patterns are shown in Fig. 1. The XRD patterns of the kaolins show identical patterns to the standards. The XRD pattern of these kaolins mineral shows impurities of quartz, calcite and others. The degree of structural disorder of the kaolinite samples can be evaluated on the basis of the XRD background in the range 2θ=20-30 °, and the width of the (002) diffraction peak d=3.58 Å at half the maximum height [40-43]. Structural order in these kaolins was estimated using the Hinckley index (HI) [41], and shown in Table 2. The Hinckley crystallinity index of kaolinite varies from area to area where the sample was collected. This variability may be attributed to differences in the geological environment such as intensity of

weathering or the extent of transportation of the minerals during formation or deposition [44]. The Hinckley crystallinity index of kaolinite varies from 0.59 (XNA-1) to 1.27(ZJK-1). It is found that kaolinite sample from Hebei Zhangjiakou is more pure and better crystalline than others, while samples from Guizhou and Hunan Xianrenwan are mainly hallosite. The chemical composition of the eight kaolins is reported in Table 3. Six kaolinite samples had similar chemical composition, as did halloysite. A comparison of kaolinite and hallosite indicates that the distribution of chemical composition in these kaolins is various. The major difference in chemical composition between kaolinite and halloysite were the Si and Al content. The chemical composition of SiO_2 is less concentrated in hallosite, but LOI is more concentrated than kaolinite.

3.2 Thermogravimetric analysis

The thermogravimetric analysis of 6 kaolinites and 2 halloysites are shown in Fig. 2. There are three main mass losses in this process. The first small mass loss is observed from 45 to 62 °C, Which is attributed to the elimination of adsorbed water molecules on the external surfaces of the kaolinite particles. Kaolinite does not present either interlayer cations or naturally intercalated water. This being the case, all mass losses at this temperature in the thermal analysis of pure kaolinite is assigned to desorption of water. This process is observed that the mass loss is about 0.5% in kaolinite and 2% in halloysite. Inspection of Fig. 2 reveals that such a phenomenon is observed for kaolin, whereas this mass loss is not obvious in the ZJK-1 kaolinite mineral sample.

In the intermediate-temperature region is located possibly the most important thermal reaction of kaolinite, the elimination of water molecules through dehydroxylation. The TG analysis of kaolinite show that the evolution of volatiles from the samples began at around 330 °C, fastest at about 450 °C, and terminated at 730 °C (Fig.2). These temperatures represent dehydroxylation of kaolinite, with the onset of the transformation to metakaolin. This process can be mostly described by the followed reactions [6, 31, 45-50]:

$$Al_2Si_2O_5(OH)_4 \rightarrow Al_2O_3 \cdot 2SiO_2 + 2H_2O$$

$$Al_2O_3 \cdot 2SiO_2 \rightarrow \frac{1}{3}(3Al_2O_3 \cdot 2SiO_2) + \frac{4}{3}SiO_2$$

It can be calculated according this formula that the theoretical mass loss value is 13.95%, which is similar to the detected mass loss of all kaolinite samples. The dehydroxylation temperature is

influenced by the degree of disorder of the kaolinite structure and the amount and kind of impurities [45, 51, 52]. Comparing the temperature of dehydroxylation (Table 2), it is established that kaolinite with lower Hinckley crystallinity index dehydroxylates at lower temperatures than those whose Hincley index are high.

The above equation is unable to describe halloysite precisely. It is noticed that the dehydration reaction in halloysite has three stages. The first mass loss step is desorption of water on the surface of particles. The second mass loss steps occur at around 225 °C for GV-1 and 223 °C for XRW-1 with a mass loss of 3.79% and 4.35%, which is attributed to the thermal dehydration of halloysite in the structural layer. The following decomposition process is similar to kaolinite. The farther mass loss of 9.61% at 425 °C for GV-1 and 9.77% at 426 °C for XRW-1 are observed, which are assigned to dehydroxylation as halloysite, which is similar to the dehydroxylation of kaolinite. The last mass loss step at 920 °C for GV-1 with a mass loss of 0.37% was observed. The most likely explanation for this mass loss is due to thermal decomposition of sulfide impurity.

3.3 Mass spectrometric analysis

It is well known that the chemical composition of kaolin is $Al_2Si_2O_5(OH)_4$. In accordance with former findings no distinct stage of dehydration has occurred (at about 450 °C). However, this are unable describe the decomposition of China kaolin exactly. Because most of kaolin in China contains a certain amount of organic. In order to clarify the decomposition mechanism of kaolin, the mass loss during each decomposition process should be characterized by the identified evolution components.

The interpretation of the mass-spectra occurs on the basis of degassing profiles from the molecule ions of water (H_2O^+: m/Z=18), carbon dioxide (CO_2^+: m/Z=44) and sulfur dioxide (SO_2^+ : m/Z=64) as well as by fragment ions (OH^+: m/Z=17 and O^+ :m/Z=16).

The evolution of gas species has been followed in situ by the coupled TG-MS system. The evolution curves of ion-fragments of various gases released are shown as ion current versus temperature curves in Figs. 3a-h. The characterization of water release by means of MS is possible with the molecule ion H_2O^+ (m/Z=18) together with the fragment ion OH^+ (m/Z=17) and O^+ (m/Z=16). Peaks at 220 and 450 °C are found in the ion current curve for H_2O^+ (m/Z=18); corresponding peaks are also found in the ion current curves for OH^+ (m/Z=17) and O^+ (m/Z=16). It can be safely concluded

that water is given out at about 220 and 450 °C from the samples, which is consistent with the mass loss observed at about 220 and 450 °C from the TG curves. The dehydration takes place in the minor step at around 225 °C, which is attributed to dehydration of the impurity of calcite. The ion fragment m/Z =16 (O^+) originates mainly from the evolution of both H_2O^+ and O_2^+. Some change in intensities of the m/Z=44 fragments was observed, probably as oxidation effect caused by the intense oxygen evolution. Basically this fragment ion indicates evolution of CO_2^+. The ion current curves for the evolved gases show for m/Z=44 a mass gain at around 225 and 350 °C, attributed to decomposes of an organic impurity (Fig. 4a). A further mass gain of CO_2 occurs at 710 °C, which assigned to decomposition of calcite. It is generally considered that the $CaCO_3$ decomposes nominally at 898 °C, but in silicate minerals generally at 600-700 °C [53, 54]. However, CO_2 is not observed in the kaolin samples ZJK-1 and XRW-1. It is thus evident that the CO_2 is from calcite. A remarkable SO_2 released in the halloysite GV-1 was observed. This may be attributed to thermal decomposition of sulfide from the presence of a sulfide impurity. The comparison of kaolinite and hallosite is shown that the thermal decomposition of kaolin is determined by different factors, such as degree of the structural ordering, mineral impurities and adsorbed and substituted ions. The mass gain in the MS curves corresponds precisely with the mass loss in the TG curves.

The present results allow making the conclusion that combination TG and MS is a powerful technique to follow the decomposition process and detect the thermal decomposition products. In the same time, it can be sassily detect the impurity in the samples which contain the carbonate and sulfide from the products of thermal decomposition. Therefore, this founding is quite important for studying minerals, especially clay minerals, because the nature clay from China always contain carbonate and sulfide component.

3.4 Scanning electron microscope (SEM)

To characterize the morphological difference among these kaolin samples, SEM images were provided. As an illustrative example, Fig. 4 displays the SEM images for six kaolinites and two halloysites. Vermicular and book-like morphology is observed in the kaolinite samples (S-1 and ZJK-1). Some large kaolinite flakes are stacked together to form agglomerates, Fig.4 a and f. These kaolinites show particles with angular edges, which suggest they are well-ordered kaolinite. Some kaolinite

175 samples (GX-1 and XNA-1) randomly distributed dislocations in the stacked layers. The HUN-1 and
176 XNA-1 have stacks of very small kaolinite particles of submicron size (Fig. 4 b and e). These kaolinites
177 are generally called “poor crystallized kaolinites”, and present much poorly built particles, which are
178 thinner and smaller than the particles from a well-crystallized mineral. Fig.4 g (GV-1) and h (XRW-1)
179 show the majority of the samples consist of cylindrical tubes of 40-50 nm diameter and length of 0.5-2
180 μm. Halloysite were usually present in curled, tublar, club-like, or mutli-layer tubular morphology.
181

182 # 4. Conclusions

183 The thermal decomposition of eight kaolins collected from different part of China has been
184 examined using TGA-MS, which is proved to be a very useful technique for determining the thermal
185 decomposition and stability of these minerals. The TG-MS have detected and monitored definitely
186 thermally evolved H_2O (m/Z=18). CO_2 (m/Z=44) and SO_2 (m/Z=64). Anyhow, the m/Z=18 is also the
187 most intense fragment of H_2O, while m/Z=44, 64 fragments arise from organic and sulfide impurities.
188 The temperature of dehydroxylation of kaolinite is influenced by the degree of disorder of the kaolinite
189 structure and the amount and kind of impurities. It is important to remark that the interlayer carbonate
190 form impurity is released as CO_2 around 225 °C, 350 °C and 710 °C in the kaolin samples (S-1, HUN-1,
191 LS-1, GX-1 and XNA-1). Thus for geosequestration decarbonization and purification before industry
192 application of kaolin is necessary. The typical morphology of kaolinite and halloysite was observed
193 to be book-like and cylindrical tubes, respectively.
194

195 # Acknowledgment

196 The authors gratefully acknowledge the financial support provided by the National “863” project of
197 China (2008AA06Z109) and infra-structure support of the Queensland University of Technology
198 Inorganic Materials Research Program of the School of Physical and Chemical Science.

References

[1] R.L. Frost, E. Mako, J. Kristof, J.T. Kloprogge, Spectrochimica Acta Part A: Molecular and Biomolecular Spectroscopy, 58 (2002) 2849-2859.

[2] F. Franco, J.A. Cecila, L.A. Pérez-Maqueda, J.L. Pérez-Rodríguez, C.S.F. Gomes, Applied Clay Science, 35 (2007) 119-127.

[3] G. Rutkai, É. Makó, T. Kristóf, Journal of Colloid and Interface Science, 334 (2009) 65-69.

[4] H.H. Murray, Applied Clay Science, 17 (2000) 207-221.

[5] C. Nkoumbou, A. Njoya, D. Njoya, C. Grosbois, D. Njopwouo, J. Yvon, F. Martin, Applied Clay Science, 43 (2009) 118-124.

[6] K. Heide, M. Foldvari, Thermochimica Acta, 446 (2006) 106-112.

[7] S. Chandrasekhar, S. Ramaswamy, Applied Clay Science, 37 (2007) 32-46.

[8] S. Zhao, T. Wang, H. Xu, Y. Guo, Feijinshukuang, 32 (2009) 37-39, 42.

[9] J.D. Miller, J. Nalaskowski, B. Abdul, H. Du, The Canadian Journal of Chemical Engineering, 85 (2007) 617-624.

[10] H.H. Murray, Clay Minerals, 34 (1999) 39-49.

[11] K.P. Nicolini, C.R.B. Fukamachi, F. Wypych, A.S. Mangrich, Journal of Colloid and Interface Science, 338 (2009) 474-479.

[12] J.E. Gardolinski, F. Wypych, M.P. Cantão, Quimica Nova, 24 (2001) 761-767.

[13] J.E. Gardolinski, H.P.M. Filho, F. Wypych, Quimica Nova, 26 (2003) 30-25.

[14] P.M. Costanzo, J. R. F. Giese, Clays and Clay Minerals, 33 (1985) 415-423.

[15] M.A. Siddiqui, Z. Ahmed, A.A. Saleemi, Applied Clay Science, 29 (2005) 55-72.

[16] S.-l. Ding, Q.-f. Liu, M.-z. Wang, Procedia Earth and Planetary Science, 1 (2009) 1024-1028.

[17] Q. Liu, D.A. Spears, Q. Liu, Applied Clay Science, 19 (2001) 89-94.

[18] F. Franco, L.A. Pérez-Maqueda, J.L. Pérez-Rodríguez, Journal of Colloid and Interface Science, 274 (2004) 107-117.

[19] X.-r. Zhang, D.-h. Fan, Z. Xu, Journal of Tongji University (Natural Science), 33 (2005) 1646-1650.

[20] E. Mako, J. Kristof, E. Horvath, V. Vagvolgyi, Journal of Colloid and Interface Science, 330 (2009) 367-373.

[21] H.H. Murray, I. Wilson, Clays and Clay Minerals, 55 (2007) 644-645.

[22] K.J.D. MacKenzie, I.W.M. Brown, R.H. Meinhold, M.E. Bowden, Journal of the American Ceramic Society, 68 (1985) 293-297.

[23] I.W.M. Brown, K.J.D. Mackenzie, M.E. Bowden, R.H. Meinhold, Journal of the American Ceramic Society, 68 (1985) 298-301.

[24] H. He, C. Hu, J. Guo, H. Zhang, Chinese Journal of Geochemistry, 14 (1995) 78-82.

[25] G.W. Brindley, M. Nakahira, Journal of the American Ceramic Society, 40 (1957) 346-350.

[26] J.G. Cabrera, M. Eddleston, Thermochimica Acta, 70 (1983) 237-247.

[27] A. Gaylord D, G. Paul D, Journal of the American Ceramic Society, 57 (1974) 132-135.

[28] J.B. Howard, K. Frank, Journal of the American Ceramic Society, 52 (1969) 199-203.

[29] J.S. Killingley, S.J. Day, Fuel, 69 (1990) 1145-1149.

[30] R.L. Frost, Clays and Clay Minerals, 46 (1998) 280-289.

[31] C.Y. Chen, G.S. Lan, W.H. Tuan, Ceramics International, 26 (2000) 715-720.
[32] R.L. Frost, M. Weier, K. Erickson, Journal of Thermal Analysis and Calorimetry, 76 (2004) 1025-1033.
[33] R.L. Frost, S. Palmer, J. Kristóf, E. Horváth, Journal of Thermal Analysis and Calorimetry, 99 (2010) 501-507.
[34] J. Dubois, M. Murat, A. Amroune, X. Carbonneau, R. Gardon, T.S. Kannan, Applied Clay Science, 13 (1998) 1-12.
[35] A.J. Locke, W.N. Martens, R.L. Frost, Thermochimica Acta, 459 (2007) 64-72.
[36] D. Galusek, Z. Lences, P. Sajgalik, R. Riedel, Journal of Mining and Metallurgy, Section B: Metallurgy, 44 (2008) 35-38.
[37] G. Meng, Z. Xu, X. Qi, W. Yang, Z. Xie, Gongye Cuihua, 15 (2007) 1-5.
[38] A. Leszczynska, K. Pielichowski, Journal of Thermal Analysis and Calorimetry, 93 (2008) 677-687.
[39] L.K. Joseph, H. Suja, G. Sanjay, S. Sugunan, V.P.N. Nampoori, P. Radhakrishnan, Applied Clay Science, 42 (2009) 483-487.
[40] G. Kakali, T. Perraki, S. Tsivilis, E. Badogiannis, Applied Clay Science, 20 (2001) 73-80.
[41] D.N. Hinckley, Clays and clay minerals, 11 (1963) 229-235.
[42] R. Vigil de la Villa, F. Moisés, S.d.R.M. Isabel, V. Iñigo, G. Rosario, Applied Clay Science, 36 (2007) 279-286.
[43] C. He, E. Makovicky, B. Osbaeck, Applied Clay Science, 9 (1994) 165-187.
[44] C.S. Manju, V.N. Nair, M. Lalithambika, Clays and Clay Minerals, 49 (2001) 355-369.
[45] P. Ptacek, D. Kubatova, J. Havlica, J. Brandstetr, F. Soukal, T. Opravil, Thermochimica Acta, In Press, Corrected Proof.
[46] O. Castelein, B. Soulestin, J.P. Bonnet, P. Blanchart, Ceramics International, 27 (2001) 517-522.
[47] Y.-F. Chen, M.-C. Wang, M.-H. Hon, Journal of the European Ceramic Society, 24 (2004) 2389-2397.
[48] R.L. Frost, H. Erzsébet, M. Éva, K. János, R. Ákos, Thermochimica Acta, 408 (2003) 103-113.
[49] S.J. Chipera, D.L. Bish, Clays and Clay Minerals, 50 (2002) 38-46.
[50] V. Balek, M. Murat, Thermochimica Acta, 282-283 (1996) 385-397.
[51] M. Földvári, Journal of Thermal Analysis and Calorimetry, 48 (1997) 107-119.
[52] L. Heller-Kallai, Journal of Thermal Analysis and Calorimetry, 50 (1997) 145-156.
[53] S. Mojumdar, Journal of Thermal Analysis and Calorimetry, 64 (2001) 1133-1139.
[54] E.T. Stepkowska, J.L. Pérez-Rodríguez, M.J. Sayagués, J.M. Martínez-Blanes, Journal of Thermal Analysis and Calorimetry, 73 (2003) 247-269.

LIST OF TABLES

Table1 Kaolin mineral samples

Kaolin Sample	Location	Content of Mineral	Impurities
Kaolinite(S-1)	Jiangsu Suzhou, China	98.6% Kaolinite	Calcite (0.5%), Quartz (0.9%)
Kaolinite(HUN-1)	Hunan, China	99% Kaolinite	Calcite (0.2%), Quartz (0.8%)
Kaolinite(LS-1)	Guangdong, China	97.4% Kaolinite	Calcite (0.3%), Quartz (2.3%)
Kaolinite(GX-1)	Guangxi, China	92% Kaolinite	Calcite (0.4%), Quartz (7.6%)
Kaolinite(XNA-1)	Anhui Huaibei, China	98.8% Kaolinite	Calcite (0.5%), Quartz (0.7%)
Kaolinite(ZJK-1)	Hebei Zhangjiakou, China	95% Kaolinite	Quartz (5%)
Halloysite(GV-1)	Guizhou, China	97.7% Halloysite	Calcite (0.3%), Gibbsite (2.0%)
Halloysite(XRW-1)	Hunan Xianrenwan, China	83.2% Halloysite	Quartz (8.1%), Gibbsite (8.7%)

Table 2 The crystallinity index of kaolinite samples

Kaolinite samples	S-1	HUN-1	LS-1	GX-1	XNA-1	ZJK-1
Hinckley index (HI)	1.04	1.0591	1.043	0.8502	1.04	1.2557
Temperature of dehydroxyl(°C)	443	449	445	435	444	464
Mass losses (%)	13.33	12.85	11.89	12.06	12.61	13.65

Table3 The chemical composition of kaolin samples

Kaolin samples	SiO_2	TiO_2	Al_2O_3	Fe_2O_3	MnO	MgO	CaO	Na_2O	K_2O	**LOI** (Loss on ignition)
S-1	**44.11**	**0.26**	**38.4**	**0.47**	**0.001**	**0.07**	**0.12**	**0.03**	**0.37**	**15.16**
LS-1	**46.34**	**0.52**	**37.67**	**0.94**	**0.003**	**0.16**	**0.06**	**0.09**	**0.31**	**13.29**
GX-1	**52.18**	**1.39**	**29.55**	**1.3**	**0.004**	**0.01**	**0.37**	**0.55**	**0.017**	**14.05**
HUV-1	**45.41**	**1.07**	**38.62**	**0.83**	**0.003**	**0.1**	**0.05**	**0.02**	**0.37**	**13.64**
XNA-1	**43.38**	**0.87**	**37.67**	**0.65**	**0.01**	**0.27**	**0.27**	**0.24**	**0.82**	**15.49**
ZJK-1	**47.05**	**1.38**	**36.33**	**0.4**	**0.004**	**0.01**	**0.47**	**0.081**	**0.01**	**13.93**
GV-1	**40.34**	**0.05**	**39.77**	**0.44**	**0.057**	**0.03**	**0.74**	**0.05**	**0.11**	**17.61**
XRW-1	**35.47**	**0.065**	**34.51**	**1.36**	**0.22**	**0.81**	**0.47**	**0**	**0.32**	**26.69**

LIST OF FIGURES

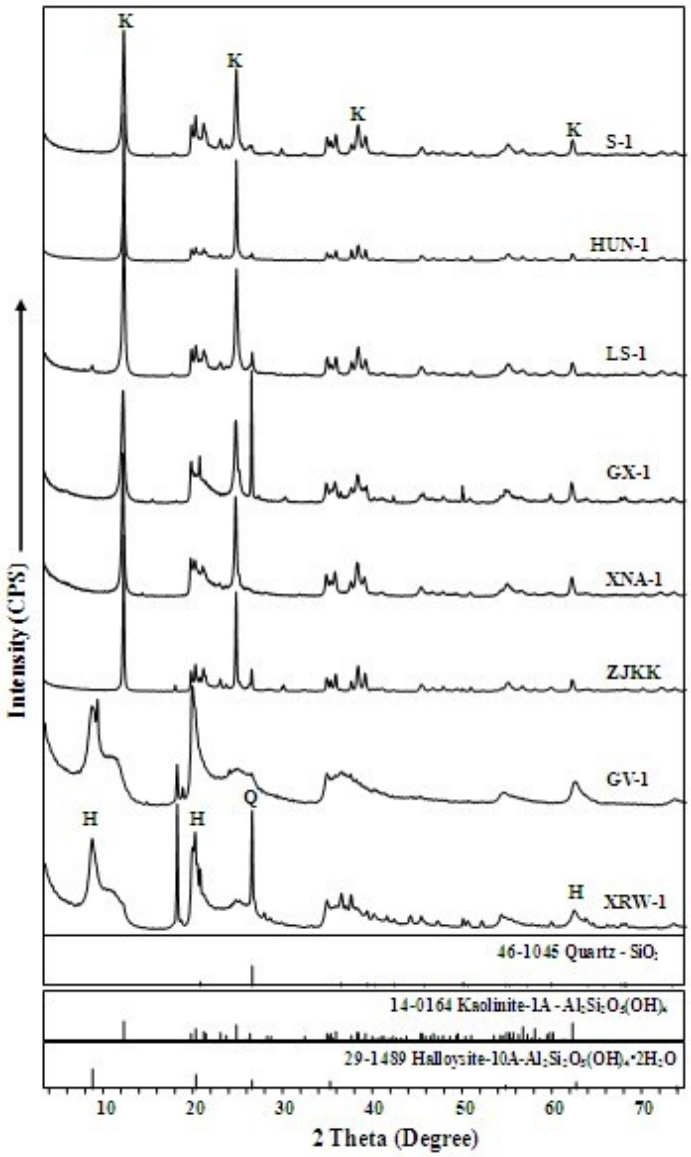

Fig.1 XRD patterns for kaolin samples (a)S-1, (b) HUN-1, (c)LS-1, (d)GX-1, (e) XNA-1, (f) ZJK-1, (g)GV-1, (h)XRW-1

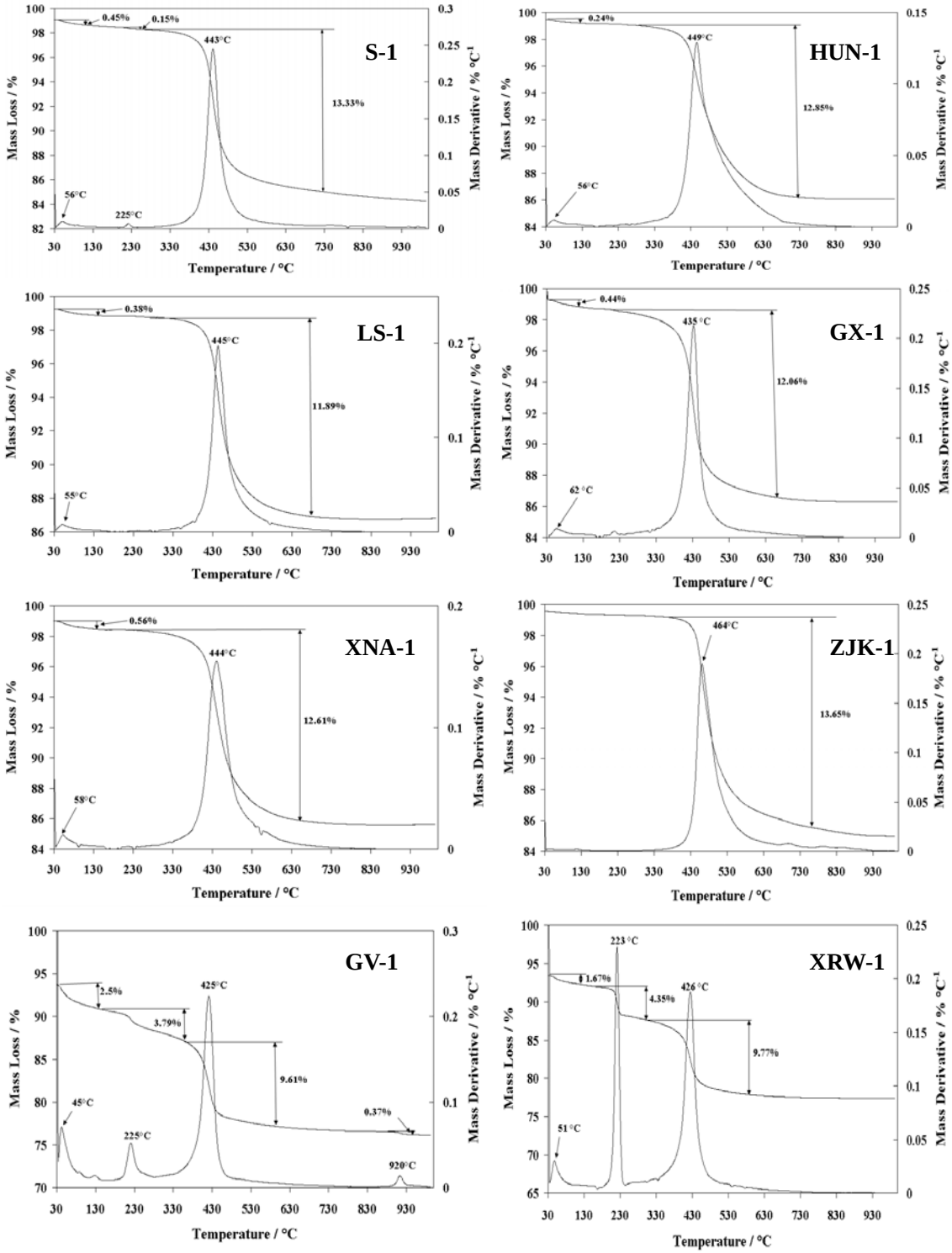

Fig.2 TGA results for kaolin samples (a)S-1, (b) HUN-1, (c)LS-1, (d)GX-1, (e) XNA-1, (f) ZJK-1, (g)GV-1, (h)XRW-1

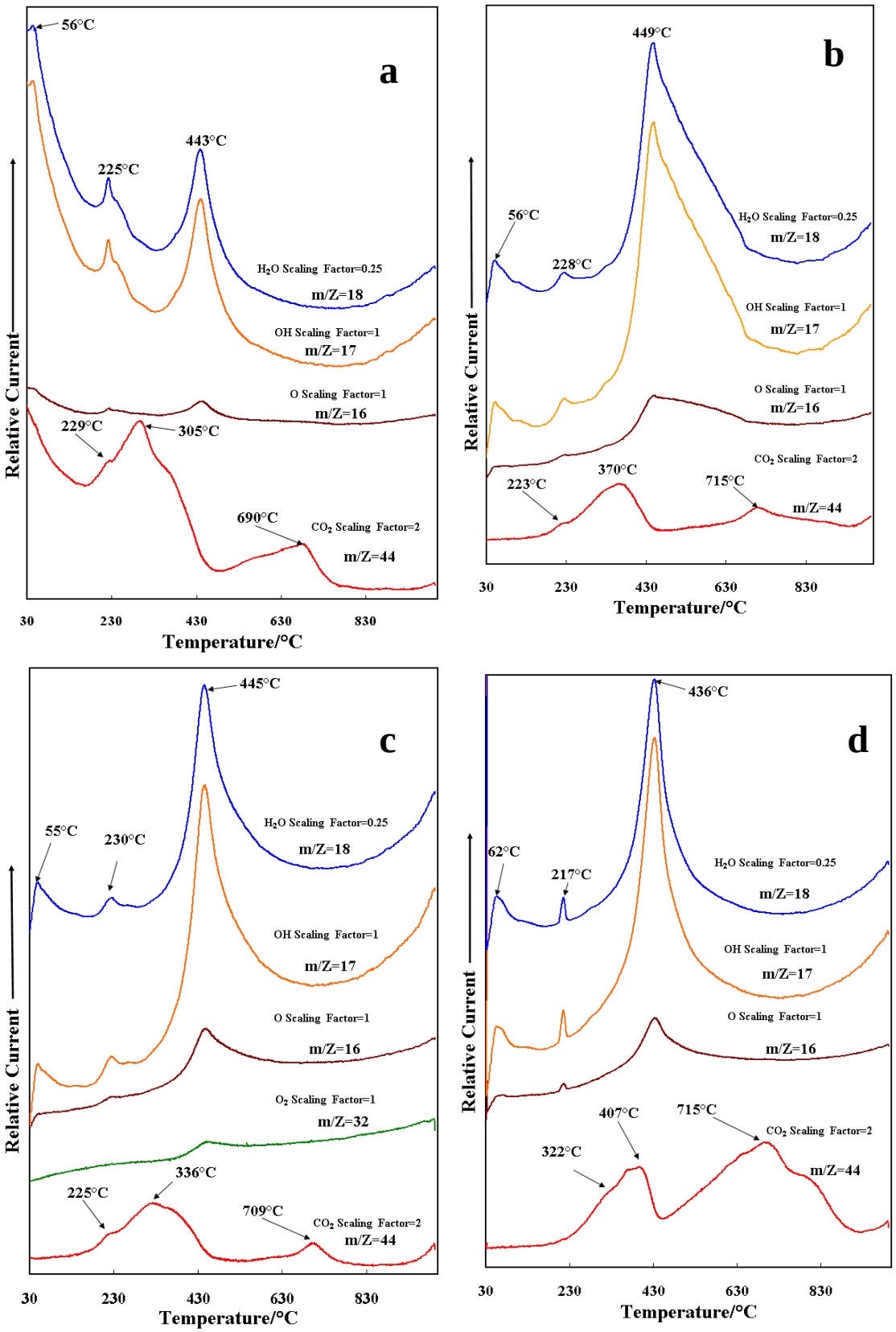
a
56°C
225°C
443°C
H2O Scaling Factor=0.25
m/Z=18
OH Scaling Factor=1
m/Z=17
O Scaling Factor=1
m/Z=16
229°C
305°C
690°C
CO2 Scaling Factor=2
m/Z=44
Relative Current
30
230
430
630
830
Temperature/°C
b
449°C
56°C
228°C
H2O Scaling Factor=0.25
m/Z=18
OH Scaling Factor=1
m/Z=17
O Scaling Factor=1
m/Z=16
CO2 Scaling Factor=2
370°C
223°C
715°C
m/Z=44
Relative Current
30
230
430
630
830
Temperature/°C
c
445°C
55°C
230°C
H2O Scaling Factor=0.25
m/Z=18
OH Scaling Factor=1
m/Z=17
O Scaling Factor=1
m/Z=16
O2 Scaling Factor=1
m/Z=32
336°C
225°C
709°C
CO2 Scaling Factor=2
m/Z=44
Relative Current
30
230
430
630
830
Temperature/°C
d
436°C
62°C
217°C
H2O Scaling Factor=0.25
m/Z=18
OH Scaling Factor=1
m/Z=17
O Scaling Factor=1
m/Z=16
407°C
715°C
CO2 Scaling Factor=2
322°C
m/Z=44
Relative Current
30
230
430
630
830
Temperature/°C

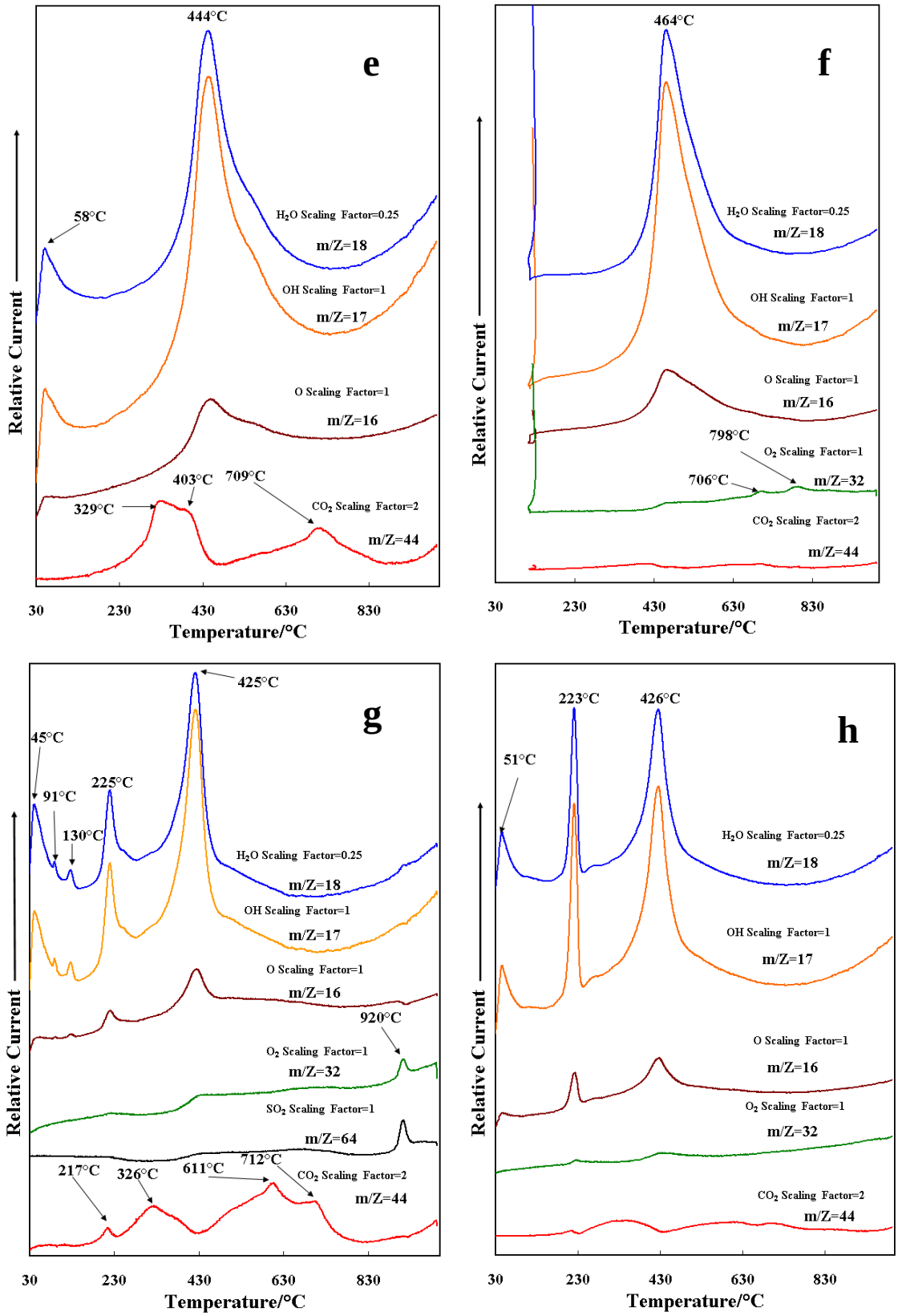

Fig.3 Evolved gas analysis for kaolin samples (a)S-1, (b) HUN-1, (c)LS-1, (d)GX-1, (e) XNA-1, (f) ZJK-1, (g)GV-1, (h)XRW-1

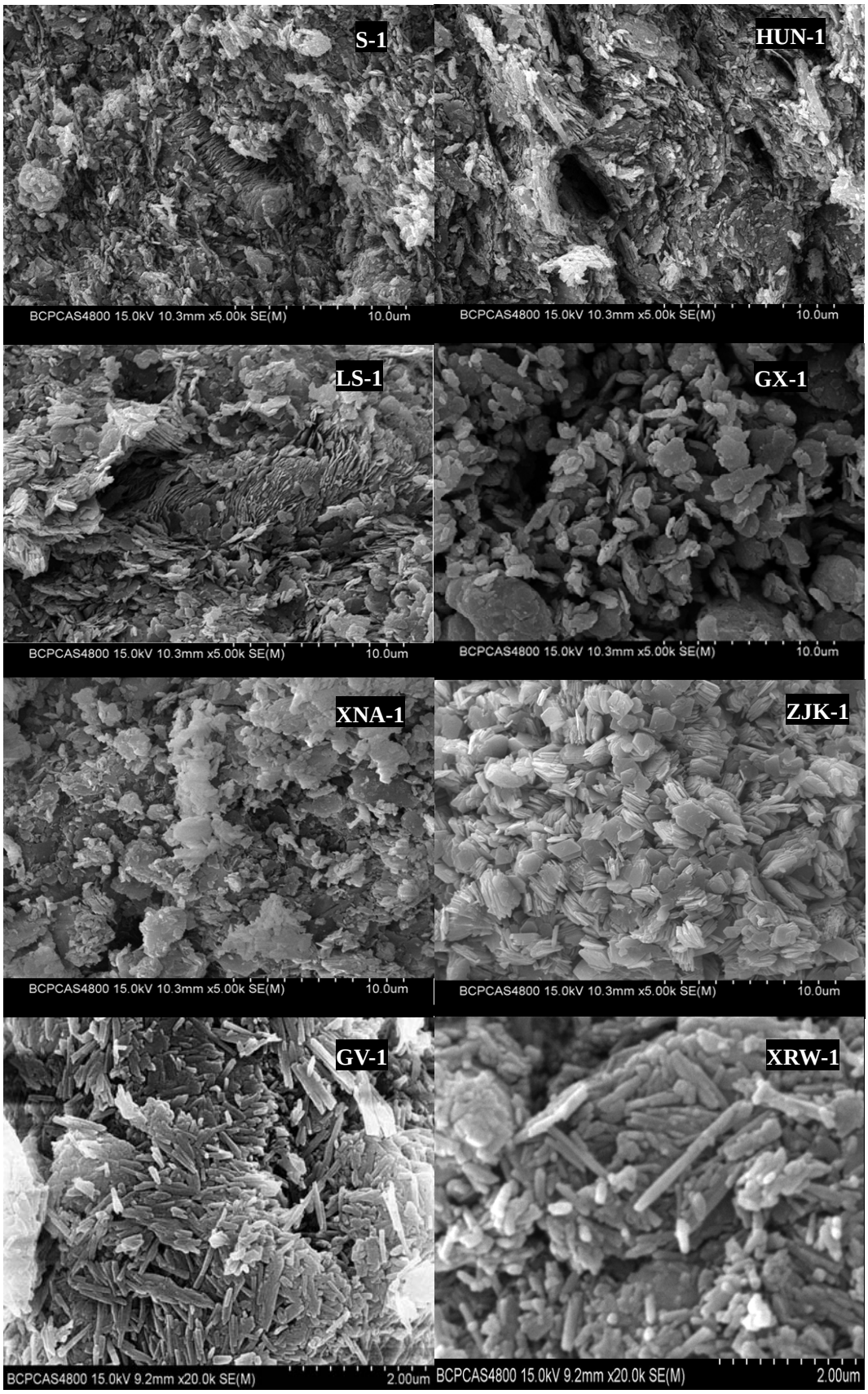

Fig.4 SEM images for kaolin samples (a)S-1, (b) HUN-1, (c)LS-1, (d)GX-1, (e) XNA-1, (f) ZJK-1, (g)GV-1, (h)XRW-1